International Journal of Thermal Sciences 156 (2020) 106434

Contents lists available at ScienceDirect

International Journal of Thermal Sciences

journal homepage: http://www.elsevier.com/locate/ijts

Influence of thermal buoyancy on vortex shedding behind a circular cylinder in parallel flow

Gazy F. Al-Sumaily [a,c,*], Hayder A. Dhahad [a], Hasanen M. Hussen [b], Mark C. Thompson [c]

[a] Workshop and Training Centre, University of Technology, Baghdad, Iraq
[b] Mechanical Engineering Department, University of Technology, Baghdad, Iraq
[c] Fluids Laboratory for Aeronautical and Industrial Research (FLAIR), Department of Mechanical and Aerospace Engineering, Monash University, Victoria, 3800, Australia

ARTICLE INFO

Keywords:
Mixed convection
Laminar parallel flow
Circular cylinder
Vortex shedding

ABSTRACT

In this study, we perform a numerical investigation to better comprehend the domination and the effect of strong thermal buoyancy on hydrodynamic and thermal characteristics, vortex shedding in particular, of a horizontal circular heated cylinder subject to a vertically upward laminar flow stream. The Reynolds number is varied in the range $20 \leq Re \leq 150$ while maintaining the Prandtl number constant at $Pr = 7.1$. The effect of thermal buoyancy on the system is determined by varying the Richardson number up to $Ri = 5$. The behaviour is determined by solving the unsteady laminar two-dimensional Navier–Stokes and standard energy equations numerically, utilising the spectral-element method with buoyancy considered using the Boussinesq approximation. Representative vorticity, streamline, and thermal patterns are presented, and the average Nusselt numbers are plotted as a function of the Richardson number for a set of Reynolds numbers to explain, in detail, the role of superimposed thermal buoyancy on the wake flow and rates of heat transfer. The predictions demonstrate that the wake flow exhibits unsteady periodic characteristics for the selected moderate Reynolds numbers, and as the buoyancy parameter increases, the fluid flow and temperature fields become less stable. Subsequently, it was observed that heat transfer augmented considerably, the vortex shedding stopped abruptly, the wake converted to steady twin vortices beyond certain critical Richardson numbers, and the Nusselt numbers suddenly reduced to minimum values. These critical values are determined to increase with the Reynolds number. The results also confirm that for increased heating, the recirculating flow in the cylinder near the wake disappears and flow separation occurs only at the backward stagnation point.

1. Introduction

One of the most interesting phenomena observed in viscous flows past bluff bodies is that of vortex shedding, with the wake structure predominantly called a von-Kármán vortex street. The characteristics of vortex shedding behind circular cylinders or similar two-dimensional obstacles have been extensively discussed; relevant reviews were provided by Bergere and Wille [1], and later by Williamson [2]. This phenomenon has significant implications for numerous thermal applications such as chimney stacks, cooling towers, fuel rods of nuclear reactors, and heat exchanger tubes, where a circular cylinder exists as one of the fundamental structural components. For applications, it must be recognised that buoyancy forces can influence the thermal and flow fields considerably under moderate Reynolds numbers and with a relatively high temperature discrepancy between the cylinder surface and flowing fluid. Indeed, the situation becomes physically complex when the heat transfer strongly influences the nature of the wake behind the hot cylinder owing to the temperature-induced buoyancy forces.

In mixed convective flows past cylinders, the heat transfer characteristics depend mainly on the Reynolds, Grashof or Richardson, and Prandtl numbers, and the angle between the forced flow and buoyancy force direction. These flows can be classified on the basis of the direction of the main flow to the buoyancy-induced flow into two primary forms, horizontal cross flows and vertical flows. In particular, the wake flow behaviour is completely different for the situation of a vertical flow under the influence of vertical buoyancy compared to that for a horizontal cross-flow configuration. The behaviour behind a circular

* Corresponding author. Workshop and Training Centre, University of Technology, Baghdad, Iraq.
E-mail addresses: gazy.alsumaily@monash.edu (G.F. Al-Sumaily), 10592@uotechnology.edu.iq (H.A. Dhahad), 20046@uotechnology.edu.iq (H.M. Hussen), mark.thompson@monash.edu (M.C. Thompson).

https://doi.org/10.1016/j.ijthermalsci.2020.106434
Received 13 March 2019; Received in revised form 9 January 2020; Accepted 17 April 2020
Available online 11 May 2020

Nomenclature

D	cylinder diameter, (m)
Gr	Grashof number, $Gr = g.\beta.D^3.(T_h - T_o)/\nu^2$
h	local convective heat transfer coefficient, $(W/m^2.K)$
k	fluid thermal conductivity, $(W/m.K)$
Nu	surface-average Nusselt number
Nu_l	local Nusselt number
Nu_m	time- and surface-average Nusselt number
p	fluid pressure, (N/m^2)
P	dimensionless fluid pressure, $P = p/\rho.v_o^2$
Pr	Prandtl number, $Pr = \nu/\alpha$
Re	Reynolds number, $Re = v_o.D/\nu$
Ri	Richardson number, $Ri = Gr/Re^2$
T	temperature, (C^o)
t	dimensionless time.
u	horizontal velocity component, (m/s)
U	dimensionless horizontal velocity component, $U = u/v_o$
v	vertical velocity component, (m/s)
V	dimensionless vertical velocity component, $V = v/v_o$
x,y	horizontal and vertical coordinates, (m)
X,Y	dimensionless horizontal and vertical coordinates, $X = x/D$, $Y = y/D$

Greek symbols

θ	dimensionless temperature, $\theta = (T - T_o)/(T_h - T_o)$
ρ	fluid density, (kg/m^3)
ν	fluid kinematic viscosity, (m^2/s)
τ	time, (s)

Subscripts

h	hot surface
o	inlet condition

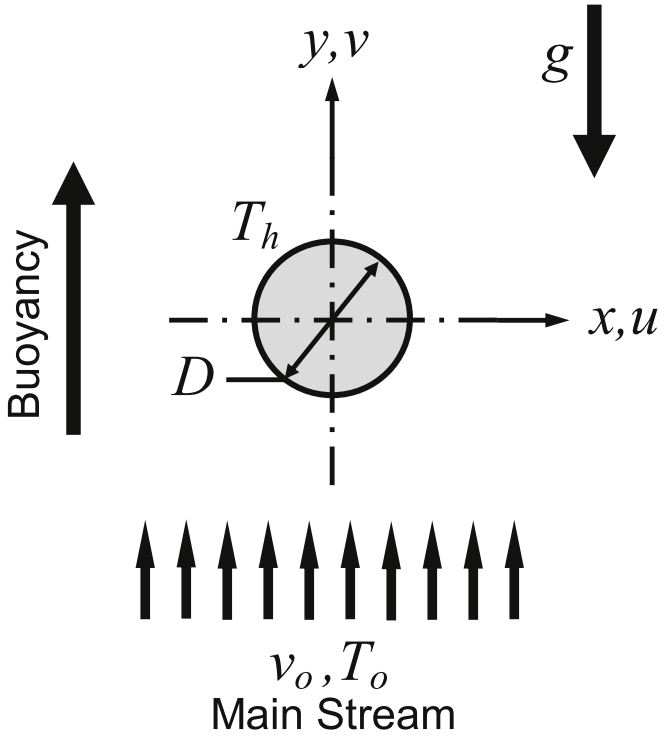

Fig. 1. Flow configuration.

cylinder within mixed convective horizontal cross flows has been reasonably studied, including in Biswas and Sandip [3], Ankit and Amit [4], Jiansheng and Yunjian [5], Jiansheng and Chen [6], Kumar and Sameen [7], Sumit and Dominic [8], Vivien et al. [9], Aleksyuk and Osiptsov [10], Amit et al. [11], Sonal et al. [12], and Zheng et al. [13].

Moreover, in a vertical flow configuration, the forced flow and buoyancy force can be in the same (*parallel-flow*) or opposing (*counter-flow*) directions. In fact, several numerical and experimental studies have been conducted previously for the situation wherein, the forced flow is pointed vertically upward (*aiding-flow*), which is the case considered in this study. Oosthuizen and Madan [14] conducted pioneering experimental work on the problem of mixed convective parallel flow for Reynolds numbers over the range $100 \leq Re \leq 300$, and proposed an empirical relationship for the Nusselt number. Jackson and Yen [15] also established a correlation that was determined to be suitable for high Grashof numbers. Other authors, for example, Acrivos [16], Joshi and Sukhatme [17], Nakai and Okazaki [18], Sparrow and Lee [19], Merkin [20], Badr [21,22], and Syakila et al. [23] numerically studied the steady-state condition of combined convection from a circular cylinder under boundary-layer flows using approximate methods. However, the aforementioned investigations were directed at studying only steady flows, disregarding the periodic flow behaviour and determining the critical Grashof number where the flow abruptly transforms from steady to unsteady.

The transient behaviour of mixed convective flow about a circular cylinder was investigated numerically by Jain and Lohar [24] and Noto and Matsumoto [25]. They revealed that the increase in the cylinder temperature increases the vortex shedding frequency. These studies, however, were performed while the flow was developing; it is not clear if they apply to a fully developed flow. Following this, Farouk and Guceri [26] analysed numerically mixed convective flow about a heated cylinder positioned between vertical parallel insulated plates for a low Reynolds number of 6.20. However, their study focused only on the effect of varying the separation distance between the plates. Ho et al. [27] reported a numerical investigation on buoyancy-aided convective flow around a cylinder placed inside an open vertical insulated duct for Reynolds numbers of 20, 40, and 60. Vortex shedding was not observed at a Reynolds number of 60, presumably owing to the considerable blockage caused by the narrow channel wall spacing. Therefore, they investigated the combined influence of the buoyancy force and channel wall spacing on the steady wake and heat transfer enhancement. It was determined that a considerable augmentation in heat transfer can be obtained through blockage variation.

Singh et al. [28] identified unsteady (full-periodic) flow and temperature fields about a hot/cold cylinder within an adiabatic vertical duct for Richardson numbers over the range $-1 \leq Ri \leq 1$, and at a fixed blockage ratio of 0.25 and Reynolds number of 100. The effect on the cylinder heating/cooling was related to the positive/negative effect of the buoyancy forces. It was demonstrated that the shedding incident persists to characterise the flow for Richardson numbers approaching 0.15; however, the aiding-buoyancy alters the dynamics entirely by stopping the shedding thereafter. They predicted that over the range $-1 \leq Ri \leq 0.15$, the increase in the magnitude of Richardson number tends to marginally decrease the average Nusselt number. However, beyond the critical value of 0.15, the increase in Richardson number serves to enhance the average Nusselt number. A similar problem was also examined by Gandikota et al. [29]. A comprehensive investigation was performed for several Reynolds numbers over the range $50 \leq Re \leq 150$, for Richardson numbers over the range $-0.5 \leq Ri \leq 0.5$, and for two

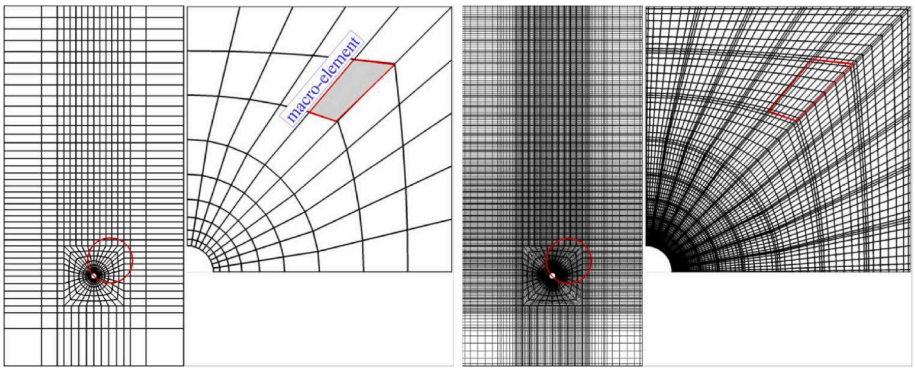

Fig. 2. Typical computational mesh employed. (Left) macro-elements, and (Right) mesh resolution enhancement by *p*-refinement with Lagrangian polynomial order of $p = 8$.

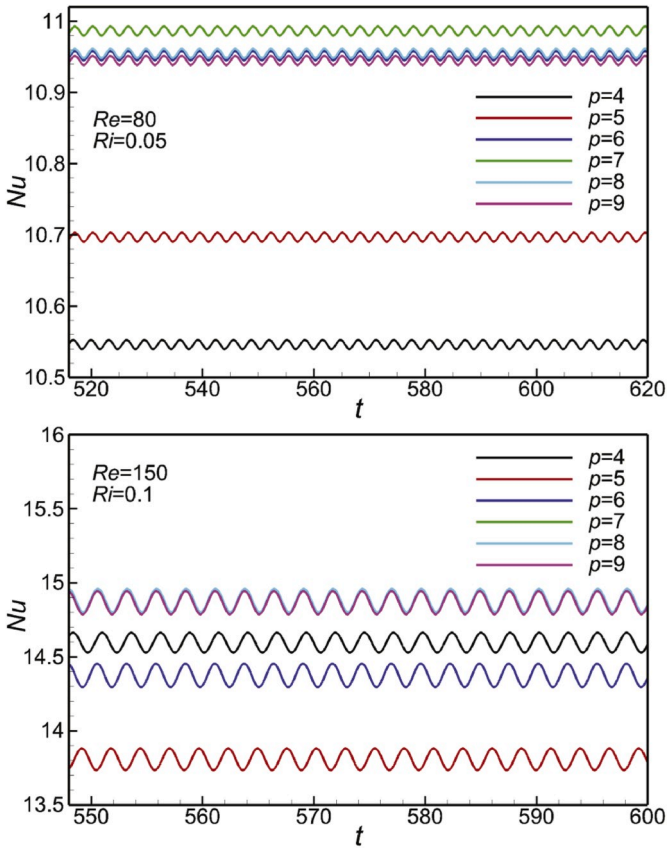

Fig. 3. Grid convergence study based on variation of average Nusselt number with time for selected Reynolds and Richardson numbers.

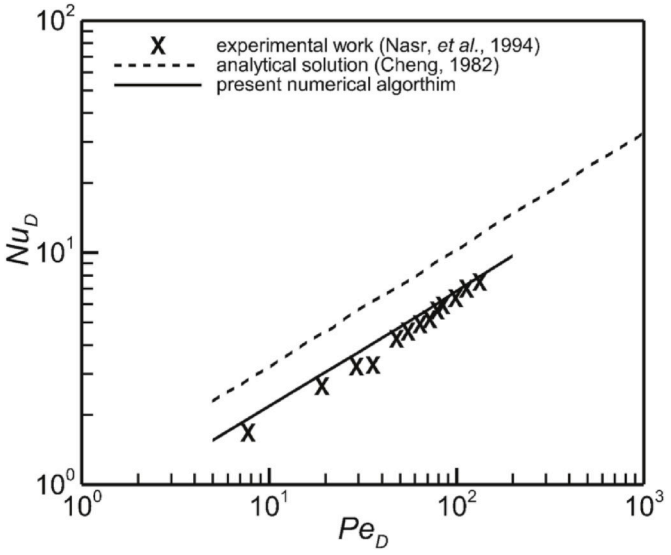

Fig. 4. Comparison between present numerical algorithm with experimental and analytical data previously reported by Nasr et al. [42] and Cheng [43].

blockage ratios of 0.02 and 0.25. For $Re = 100$, their results indicated that wake unsteadiness stops entirely at critical Richardson numbers of 0.15 and 0.18 at the above mentioned blockage parameters, with a higher critical value for the lower blockage ratio. They indicated that the proximity of the side wall restricts the fluid flow neighbouring the cylinder, which stabilises against the tendency to shed vortices, and consequently lower cylinder heating is necessitated to stabilise the flow. Remarkably, the average Nusselt number was found to persistently increase with Richardson number over its entire negative and positive ranges in both channels with a lesser gradient below the critical value.

The current literature reveals that only two studies, Chang and Sa [30] and Hatanaka and Kawahara [31], have investigated full-periodic parallel flows (*aiding-flows*) over a circular cylinder in the absence of side walls (unconfined flows). They analysed the behaviour of near-wake vortices behind a hot and/or cold circular cylinder for Richardson numbers over the range $-1 \leq Ri \leq 1$ and for a constant Reynolds number of 100. These studies used different numerical methods; however, both predicted that the cooling of the cylinder surface strengthens the shear layer and the periodic flow becomes more activated. However, heating was found to suppress the frequent flow into a stable twin-eddy structure at a critical Richardson number of 0.15, identifying a collapse of the Kármán vortex street. Hatanaka and Kawahara [31] did not document the heat transfer enhancement/diminution, as their focus was only on the changing dynamic and thermal patterns. Surprisingly, Chang and Sa [30] reported that the trend of the average Nusselt number demonstrated interesting and sensitive features in the unsteady flow region before the suppression of the vortex shedding. Thus, in the negative range of the Richardson numbers $-1 \leq Ri < 0$, the average Nusselt number increases notably; however, in the positive range of the Richardson numbers $0 < Ri < 0.15$, it decreases marginally to compose a localised minimum prior to the discontinuity at $Ri = 0.15$. Moreover, in the region of steady flow with twin stationary vortices connected to the cylinder, for $Ri \geq 0.15$, the average Nusselt number was demonstrated to increase again.

In the aforementioned investigations of Singh et al. [28], Gandikota et al. [29], and Chang and Sa [30], there are apparently conflicting conclusions concerning the reliance of the wall convective heat transfer on the Richardson number in the unsteady flow regime, where the flow

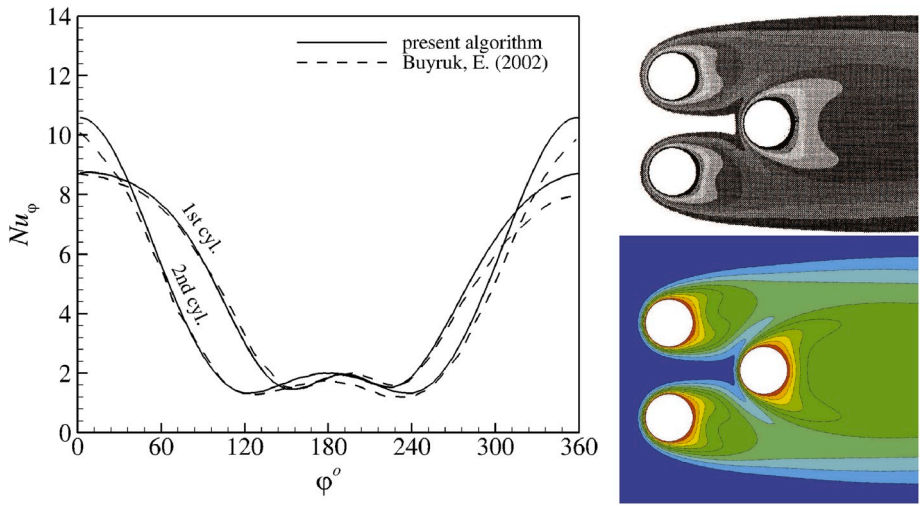

Fig. 5. Comparison between the present numerical algorithm and that one used by Buyruk [44]. (Left) for local Nusselt number distribution around first and second rows, and (Right) for thermal contours predicted by (Top) Buyruk [44] and (bottom) present code.

structure is dynamically altered and characterised by the vortex shedding. Therefore, the first objective of the current study is to investigate thoroughly the effect of this parameter, and provide a deeper understanding of the augmentation or diminution of the convective heat transfer with the Richardson number, with special attention near its critical value. Secondly, the role of the Reynolds number was ignored in these investigations. Importantly, a higher critical Richardson number could occur at a higher Reynolds number, or vice versa. This could be an indication that the critical Richardson number is not a universal property for the suppression of vortex shedding; rather, it could be Reynolds number dependent. Furthermore, after the stage of shedding suppression, stable twin vortices are formed and attached to the aft of the cylinder. A complete picture and detailed information regarding the dependency of the Nusselt number on the decaying and then vanishing of these dual vortices by the heating effect have not been provided satisfactorily. For these reasons, the present study further investigates and analyses the transient buoyant upward flows over a heated unconfined circular cylinder to better realise the connection between the temperature-induced buoyancy forces and vortex shedding patterns changing in the combined forced and free convection regime, destruction of stable wakes by the heating influence, and the convection heat transfer characteristics, for different Reynolds numbers.

2. Physical problem and governing equations

The schematic configuration of the physical problem considered in the present investigation accompanied by the Cartesian coordinate system employed are displayed in Fig. 1. The system is comprised of a stationary unconfined horizontal circular cylinder of diameter D heated to and maintained at a fixed and steady temperature T_h. The cylinder is placed within a vertical upward laminar cold free flow stream of temperature T_o and velocity v_o. The oncoming cold flow interacts with the buoyancy-driven flow from the hot exterior of the cylinder to yield a wake subject to mixed convection. The cylinder is presumed to be sufficiently long in the span-wise direction and consequently the ending influences can be ignored. Thus, the flow can be considered two-dimensional, consistent with the low Reynolds numbers of the current study. To formulate the physical problem, it is assumed that the flow is unsteady and laminar, and the fluid under consideration is incompressible and viscous. The Boussinesq approximation was used to model the thermal buoyancy effects. All the physical properties of the fluid are assumed to be invariable except for the density through the buoyancy expression, which is assumed to alter with the temperature. Although it is generally true that viscosity is a function of temperature, this is ignored in the current analysis. The dimensionless format of continuity, Navier–Stokes, and standard energy equations can be expressed in Cartesian coordinates as follows:

$$\left(\frac{\partial U}{\partial X}+\frac{\partial V}{\partial Y}\right)=0, \tag{1}$$

$$\frac{\partial U}{\partial t}+\left(U\frac{\partial U}{\partial X}+V\frac{\partial U}{\partial Y}\right)=-\frac{\partial P}{\partial X}+\frac{1}{Re}\left(\frac{\partial^2 U}{\partial X^2}+\frac{\partial^2 U}{\partial Y^2}\right), \tag{2}$$

$$\frac{\partial V}{\partial t}+\left(U\frac{\partial V}{\partial X}+V\frac{\partial V}{\partial Y}\right)=-\frac{\partial P}{\partial Y}+\frac{1}{Re}\left(\frac{\partial^2 V}{\partial X^2}+\frac{\partial^2 V}{\partial Y^2}\right)+\frac{Gr}{Re^2}\ \theta, \tag{3}$$

$$\frac{\partial \theta}{\partial t}+\left(U\frac{\partial \theta}{\partial X}+V\frac{\partial \theta}{\partial Y}\right)=\frac{1}{Re.Pr}\left(\frac{\partial^2 \theta}{\partial X^2}+\frac{\partial^2 \theta}{\partial Y^2}\right), \tag{4}$$

where U and V are the dimensionless horizontal and vertical velocities in the X and Y directions, respectively; P and t are the dimensionless pressure and time; and θ is the dimensionless temperature. These above dimensionless variables are assigned as:

$$U=\frac{u}{v_o}, V=\frac{v}{v_o}, X=\frac{x}{D}, Y=\frac{y}{D}, P=\frac{p}{\rho v_o^2}, t=\frac{\tau}{v_o D}, \theta=\frac{T-T_o}{T_h-T_o}, \tag{5}$$

where the analogous dimensional quantities are indicated by u, v, x, y, p, τ, and T, respectively. The main dimensionless pertinent parameters that could be of interest for this type of flow are Re, Gr, and Pr, which are the Reynolds, Grashof, and Prandtl numbers, respectively, and are expressed as:

$$Re=\frac{v_o D}{\nu}, Gr=\frac{g\beta D^3(T_h-T_o)}{\nu^2}, Pr=\frac{\nu}{\alpha}. \tag{6}$$

Here, ρ, α, and ν describe the fluid properties, which are the density, thermal diffusivity, and kinematic viscosity, respectively, with g and β being the gravitational acceleration and volumetric expansion coefficient.

The dimensionless initial and boundary conditions are given as follows. Initial values: the velocity and temperature variables are set initially (at $t = 0$) to zero, ($U = V = \theta = 0$). For ($t > 0$): At the inlet, a uniform upward vertical flow with velocity components ($U_o = 0$ and $V_o = 1$) is applied with the temperature set to zero ($\theta_o = 0$). At the exit plane, zero normal gradient conditions are applied for all variables ($\partial U/\partial Y = \partial V/\partial Y = \partial\theta/\partial Y = 0$). On the cylinder surface, a no-slip status ($U = V = 0$) with a consistent temperature ($\theta_h = 1$), are enforced. On the lateral confining borders, symmetry conditions modelling a frictionless

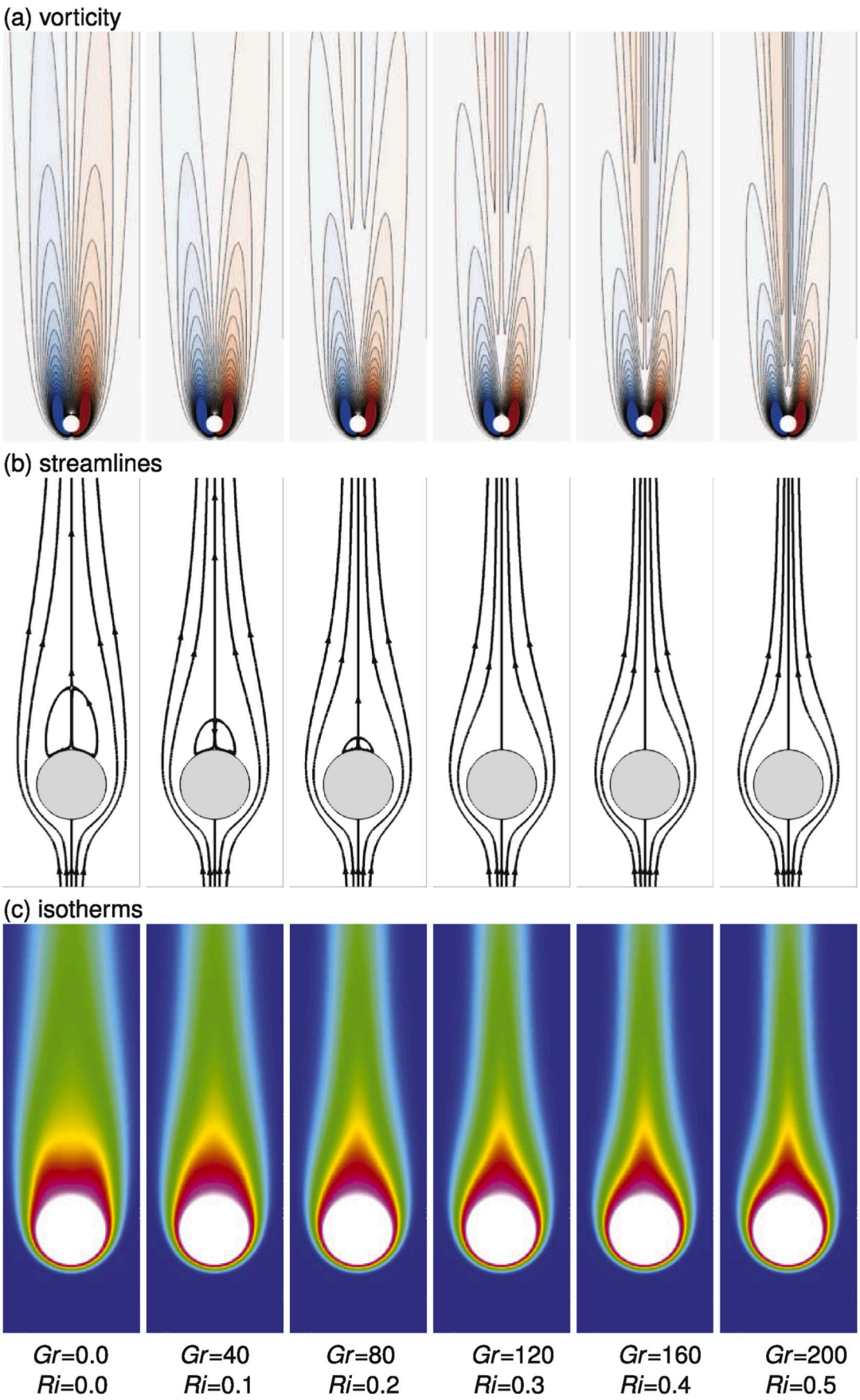

Fig. 6. (a) Vorticity, (b) streamlines, and (c) isotherm patterns for steady flow for $Re = 20$, and at different Grashof number and/or Richardson number.

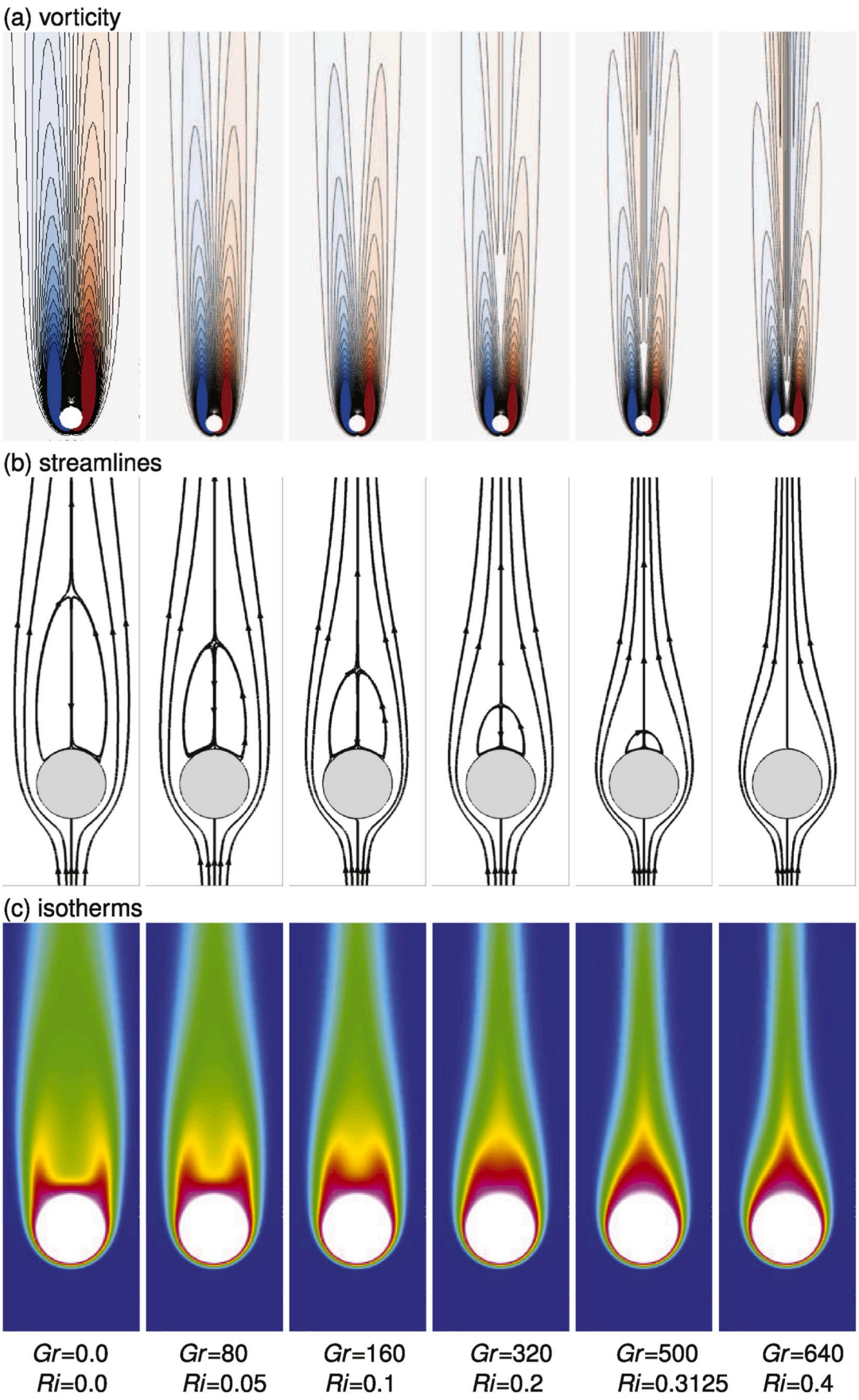

Fig. 7. (a) Vorticity, (b) streamlines, and (c) isotherm patterns for steady flow for $Re = 40$, and at different Grashof number and/or Richardson number.

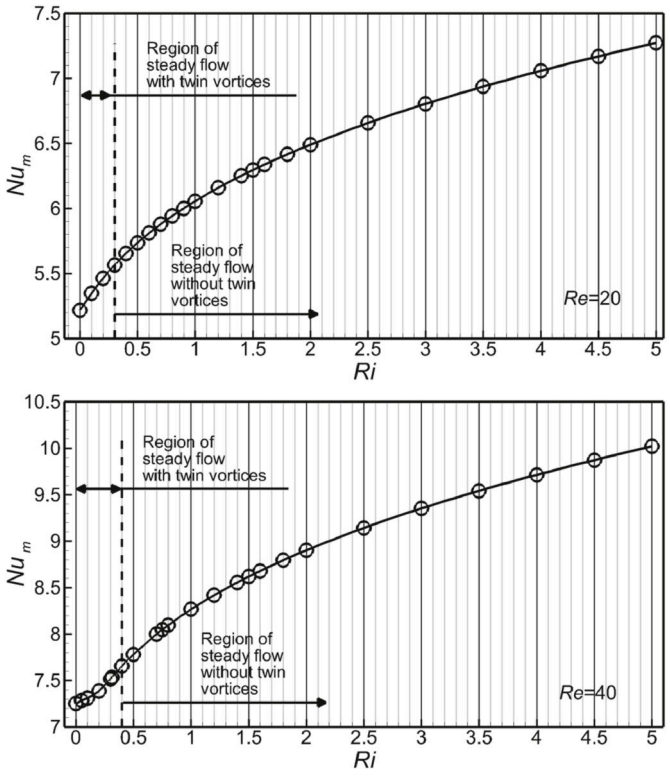

Fig. 8. The variation of time-mean surface-averaged Nusselt number versus Richardson number for $Re = 20$ and 40.

boundary ($\partial U/\partial X = V = 0$) with no heat flux ($\partial\theta/\partial X = 0$), are imposed. The flow is started impulsively from rest. The heat exchange between the hot cylinder wall and adjacent cold fluid is determined by the local Nusselt number Nu_l. Once the temperature distribution around the cylinder is determined, this dimensionless quantity is evaluated by the following formula:

$$Nu_l = \frac{hD}{k} = -\frac{\partial\theta}{\partial n}. \tag{7}$$

Here, k is the thermal conductivity of the fluid, h is the local convective heat transfer coefficient, and n is the normal distance on the cylinder wall. Subsequently, the local Nusselt number is integrated along the cylinder circumference to compute the surface-averaged heat transfer Nu. Then, the time-mean and surface-average Nusselt number, Nu_m, is calculated by integrating over a long time period.

3. Numerical method

Artificial boundaries are positioned at the ends of the computational domain forcing the blockage ratio of the cylinder diameter to the domain width equal to 1/30. The downstream and upstream of the computational domain from the cylinder centre are fixed in this investigation at 45D and 15D, respectively. These values are selected to minimise the impact of the inlet and outlet boundaries on the hydrodynamic/thermal fields in the proximity of the cylinder. An existing in-house solver was used for conducting the numerical simulations by discretising and integrating the time-dependent governing equations ((1)–(4)) for the velocity and temperature fields employing the time-splitting space spectral-element method as explained in detail by Karniadakis and Triantafyllou [32], Tomboulides et al. [33], and Thompson et al. [34].

To solve the governing equations, they must be discretised in both space and time. As indicated, the temporal discretisation employs the time-splitting of the fractional step method (see Peskin [35]). Each term

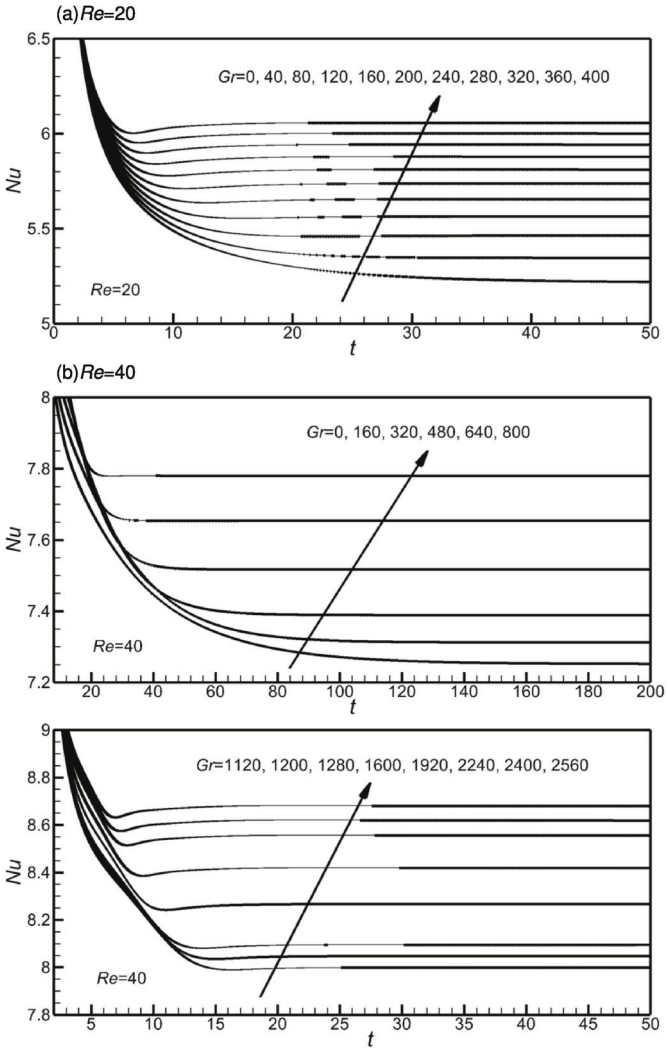

Fig. 9. Temporal surface-averaged Nusselt number of steady flows for (a) $Re = 20$ and (b) $Re = 40$, at different Grashof numbers.

on the right-hand side of the Navier–Stokes and energy equations are integrated forward in time by three and two sequential sub-steps, respectively. For the momentum equations, these steps address the advection, pressure, and diffusion terms. The sub-steps employ a variety of temporal discretisation. For example, an explicit technique (Adams-Bashforth) is employed for addressing the advection term because of its nonlinear nature, whereas an implicit method (Adams--Moulton) is employed for both the diffusion and pressure sub-steps.

Spatial discretisation is implemented using a nodal-based spectral-element technique. This is a method from the finite-element class, where the computational region is divided coarsely into a series of macro-elements. A typical two-dimensional spectral-element mesh that consists of (884) macro-elements and (958) nodes is displayed in Fig. 2 (Left). This macro-element mesh can be refined in areas of the domain that experience high gradients. This is known as an h-refinement. For the method employed herein, it is also necessary that all elements are quadrilateral, although they are free to have curved sides. Moreover, high-order Lagrangian polynomial interpolants are employed in each element to calculate the solution variables in every direction. The order of these polynomials (p) can be varied at runtime to adjust the spatial resolution. This is known as a p-refinement. This, coupled with the h-refinement, leads to the h-p Galerkin finite-element method documented in Karniadakis and Sherwin [36].

Simulations were performed to ensure that the computational pre-

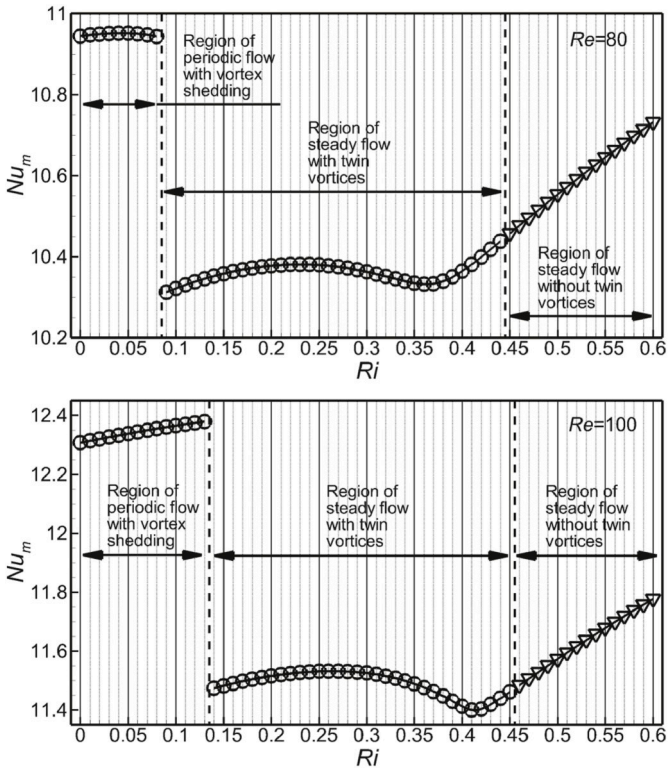

Fig. 10. Time-mean and surface-average Nusselt number versus Richardson number for $Re = 80$ (Top) and $Re = 100$ (Bottom).

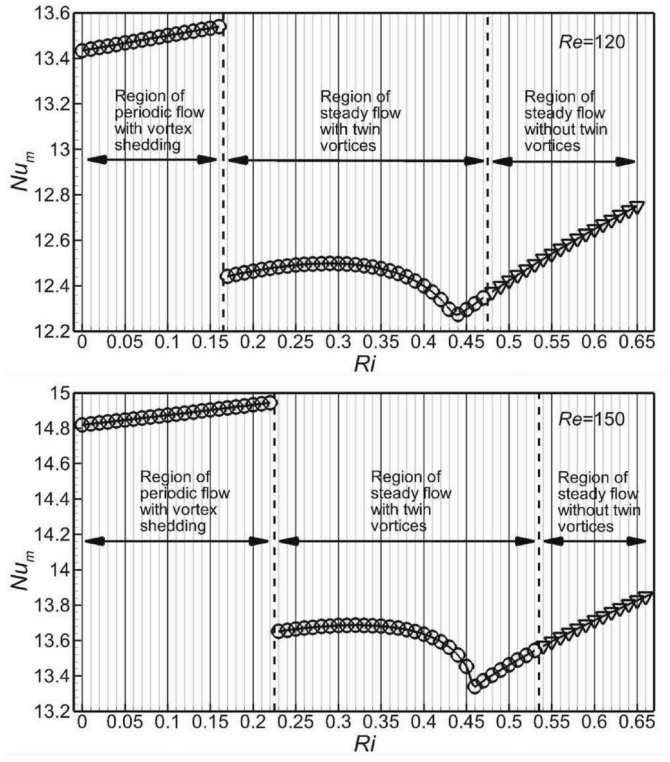

Fig. 11. Time-mean and surface-average Nusselt number versus Richardson number for $Re = 120$ (Top) and $Re = 150$ (Bottom).

dictions obtained were unrelated to the spatial grid size. Thus, a grid resolution study (*GRS*) was conducted for the configuration depicted in Fig. 1 for different relevant parameters by changing the Lagrangian polynomial, p, between four and nine, and the temporary surface-average Nusselt number Nu was observed as an indicator of convergence. For brevity, samples of the results are illustrated in Fig. 3 for two cases. The first case is for Reynolds number $Re = 80$ and Richardson number $Ri = 0.05$; the second case is for Reynolds number $Re = 150$ and Richardson number $Ri = 0.1$. The *GRS* results indicate, and one can observe in Fig. 3, that Nu is converged by $p = 8$ with less than a 1% error. Therefore, for the present numerical investigation, the Lagrangian polynomial order of $p = 8$ was utilised. Fig. 2 (Right) demonstrates the mesh resolution enhancement by p-refinement with Lagrangian polynomial order of $p = 8$.

The current implementation was validated for related problems such as circular cylinder wakes by Thompson et al. [37], forced convective flows over a single circular cylinder by Al-Sumaily et al. [38] and Al-Sumaily and Thompson [39] and over multi-cylinders by Al-Sumaily [40], and for the case of natural convective flows around a circular cylinder by Al-Sumaily and Thompson [41]. Further validations for the implementation of the present code were conducted. Results from the code were compared with the experimental and analytical data previously reported by Nasr et al. [42] and Cheng [43], respectively, and are displayed in Fig. 4. This was for the problem of convection heat transfer from an unconfined circular cylinder of diameter $D = 2.7\ mm$, embedded in a packed bed of aluminium spheres with $d_p = 12.23\ mm$. Furthermore, other numerical results were compared with those obtained by Buyruk [44] for predicting convective flow over three unbounded circular cylinders in a staggered arrangement at Reynolds number $Re_D = 80$, and at longitudinal and transverse pitches $p_l = p_t = 2$ as illustrated in Fig. 5. It can be observed in Figs. 4 and 5 that these comparisons for the variation of average and local Nusselt number and thermal patterns indicate clearly acceptable agreement between the present code and the three experimental, analytical, and numerical results.

4. Results and discussion

In the current computational investigation, laminar mixed convection heat transfer out of a heated horizontal unconfined circular cylinder is investigated within a parallel flow regime, such that the buoyancy forces and forced flow are in the same orientation, i.e. the forced flow is vertically upward directed. In this investigation, the Reynolds number is over the range $20 \leq Re \leq 150$, at several values of Grashof number (Gr) for each case; hence, the Richardson number ($Ri = Gr/Re^2$) is changed between zero and five. The positive Richardson number in equation (3) signifies that the buoyancy force is in the same direction as the fluid flow, e.g. under an *aiding buoyancy* condition. Water ($Pr = 7.1$) is used as the working fluid for the current study. It is recognised that for a circular cylinder in freestream flow, with its temperature equal to the freestream temperature, periodic shedding occurs beyond a critical Reynolds number of approximately $Re_{crit} = 46$, Williamson [2], Noto and Nakajima [45], Zdravkovich [46], and Dusek et al. [47]. Below this, a pair of symmetric vortices is generated and the flow evolves to a steady state. The vorticity, streamline, and thermal patterns for two conditions of steady flow at $Re = 20$ and 40 for Richardson numbers over the range $0 \leq Ri \leq 0.5$ are displayed in Figs. 6 and 7. For the vorticity plots, blue indicates negative vorticity or clockwise fluid rotation, whereas red indicates positive vorticity or counterclockwise rotation. For the isotherm plots, red/blue indicate hot/cold fluid. It is indicated in these figures that the cylinder wall behaves as a vorticity source by producing two zones of vorticity with reverse-sign rotation at the value of $Ri = 0$ that corresponds to pure forced convection flow in the loss of buoyancy.

The streamline plots demonstrate that the flow superficially resembles potential flow as the value of the Richardson number increases. Regarding the isothermal case, the vortex pair recirculation zone exists in the near wake of the cylinder. Furthermore, the separation of the flow occurs as the fluid passes over the side of the cylinder, and twin

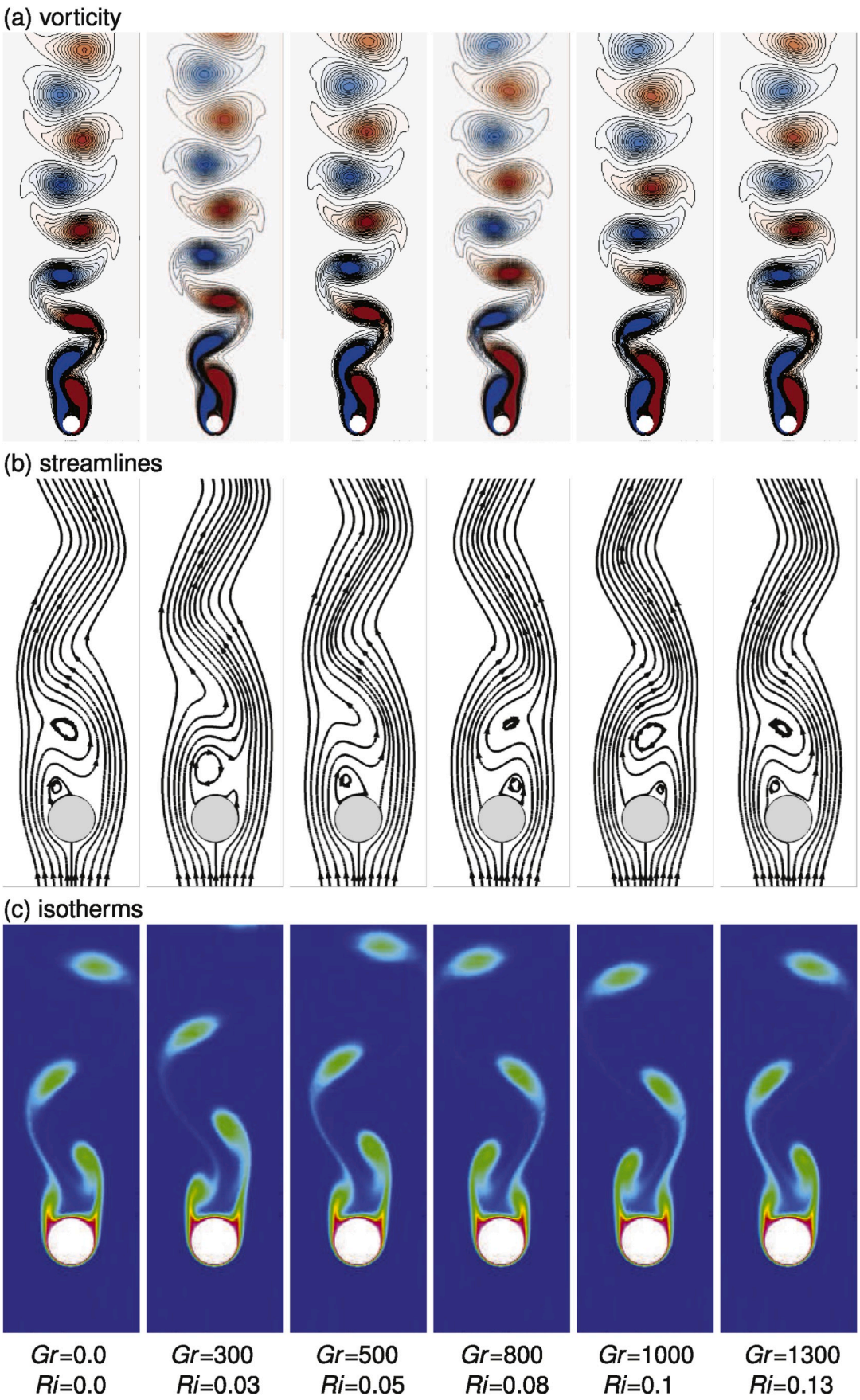

Fig. 12. (a) Vorticity, (b) streamline and (c) isotherm patterns for periodic flow with vortex shedding for $Re = 100$, at different Grashof number and/or Richardson number.

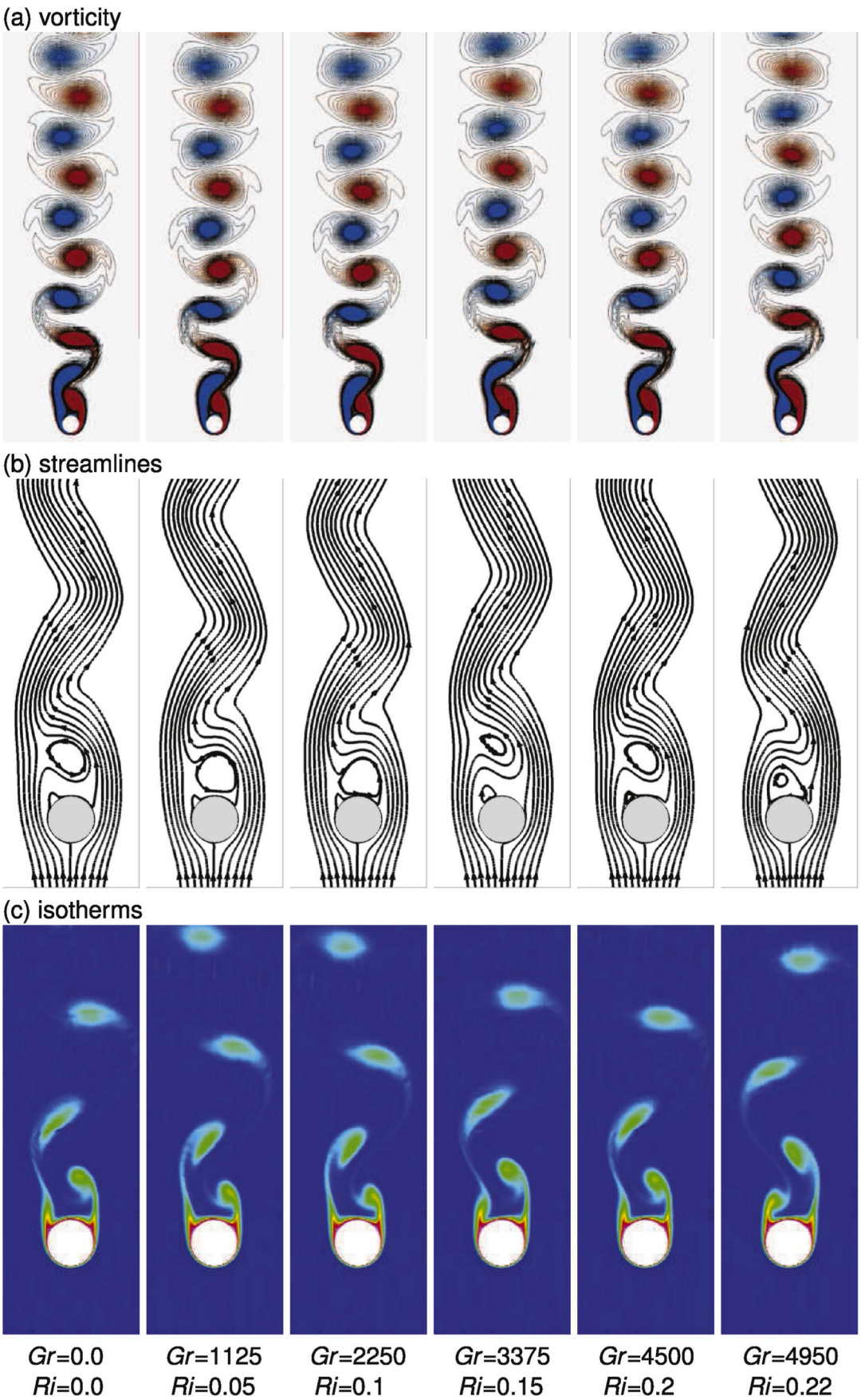

Fig. 13. (a) Vorticity, (b) streamline and (c) isotherm patterns for periodic flow with vortex shedding for $Re = 150$, at different Grashof number and/or Richardson number.

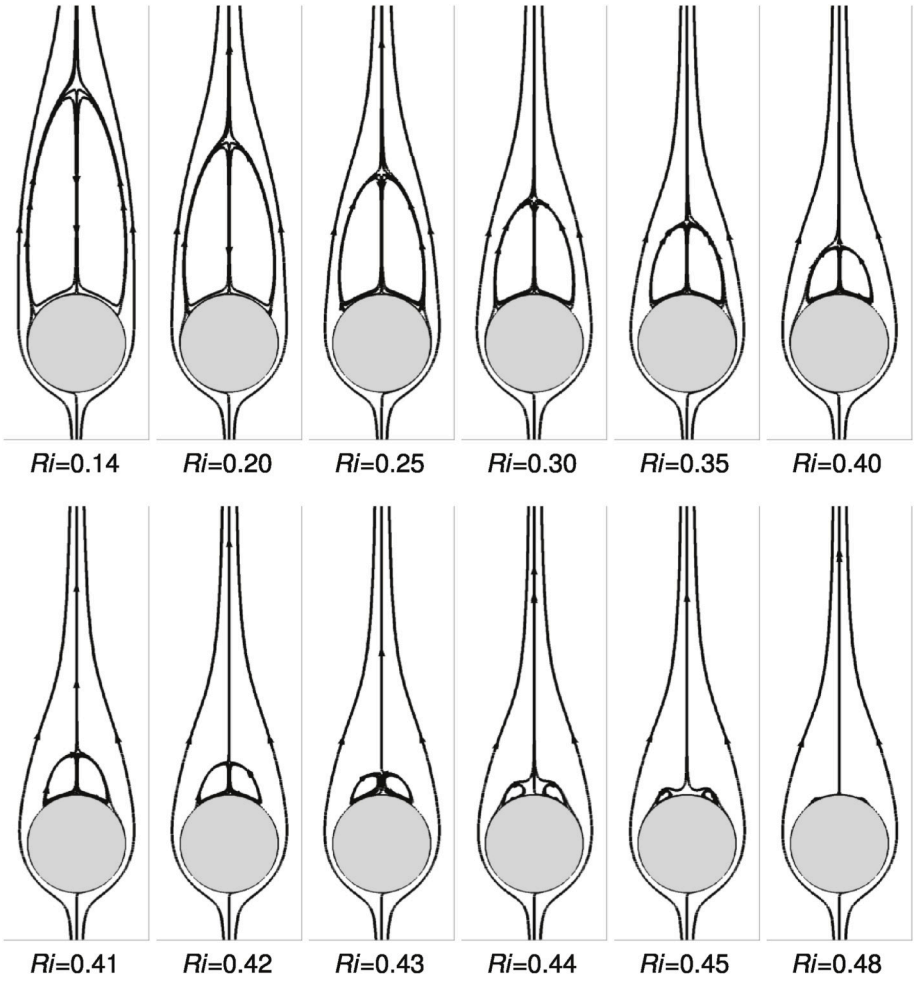

Fig. 14. Streamlines of steady flows with twin vortices for $Re = 100$, at different Richardson number.

stationary eddies known as Föppl vortices are formed. It can be observed that the two attached eddies fed from the circulation from the shear layers are symmetric with opposite-signed circulation. Moreover, the figure indicates that as the Richardson number increases, the recirculation zone progressively shortens until it entirely disappears by $Ri = 0.3$ and 0.4 for.

$Re = 20$ and 40, respectively. This is primarily because of the fact that under these aiding buoyancy circumstances, in the vicinity of the cylinder, increasing buoyancy causes the boundary layer flow to accelerate past the normal separation points, thereby delaying separation. The topological change of the vortex pair to the no-pair state is disclosed in these streamline plots. The isotherm patterns for the same cases indicate that the plume is formed in the wake region as the flow reversal is suppressed. It is also indicated that as the Richardson number increases, the lines of the thermal boundary move towards the cylinder wall, which points to a higher temperature gradient, and consequently, superior heat transfer rates are obtained. The figures clearly illustrate the dependence of the flow and thermal fields not only on the Richardson number but also on the value of the Reynolds number.

The variation of the time-mean surface-averaged cylinder Nusselt number (Nu_m) with Richardson number is plotted in Fig. 8 for two cases of $Re = 20$ and 40. The two plots are separated into two regions; the region of steady flow with the presence of twin vortices behind the cylinder (for $Ri < 0.3$ at $Re = 20$ and for $Ri < 0.4$ at $Re = 40$) and the region of steady flow without the presence of twin vortices (for $Ri \geq 0.3$ at $Re = 20$ and for $Ri \geq 0.4$ at $Re = 40$). These regions are indicated to show the change in values of Nu_m before and after the limits of disappearing of the recirculation zones at each Reynolds number. Thus, in each plot at constant Reynolds number, it can be clearly observed that the influence of the heating effect (Ri) is to significantly continuously increase Nu_m even after disappearing the two eddies attached to rear area of the cylinder. Moreover, in both cases, the plots show that the higher rates of heat transfer represented by Nu_m are found to be for higher Reynolds number.

To provide a more detailed quantification of the overall heat transfer characteristics, the distribution of the temporal averaged Nusselt number (Nu) is of practical interest. Fig. 9 (a) and (b) display the time responses of Nu following the abrupt increase in the cylinder's temperature for $Re = 20$ and 40, respectively, and for the cases of mixed and purely forced convection regimes with diverse values of the Grashof number. It can be observed that the maximum value of Nu occurs immediately after heating the cylinder because the thickness of the thermal boundary layer is small. With increasing time, the thermal boundary layer grows and Nu reduces and approaches an asymptotic state. Furthermore, it can be observed that the steady-state condition of Nu approaches more quickly as the heating or Grashof number is increased and/or the Reynolds number is decreased.

Attention is next focused on the influence of thermal buoyancy forces on the periodic flow behaviour and thermal characteristics, and in particular, on the vortex shedding that occurs for Reynolds numbers beyond the critical value. Hence, further numerical investigations were conducted for the cases of $Re =$

80, 100, 120, and 150, addressing a wide range of Richardson number for each case. The reaction of the time-mean surface-averaged Nusselt number to the increase in natural convection over the forced flow is illustrated in Figs. 10 and 11. The graphs in these figures indicate

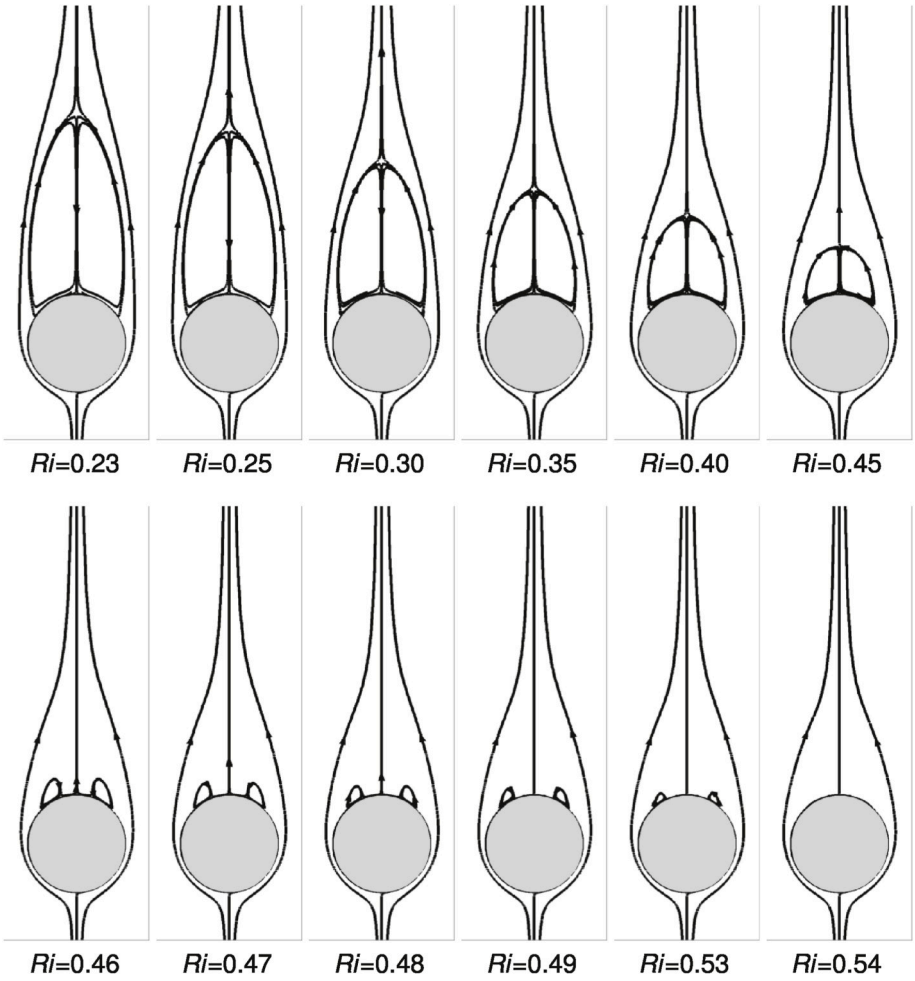

Fig. 15. Streamlines of steady flows with twin vortices for $Re = 150$, at different Richardson number.

interesting features for the variation of the time-mean surface-averaged cylinder Nusselt number with the Richardson number. They indicate that this distribution can be divided into three regions: Periodic flow with vortex shedding, steady flow with twin vortices, and steady flow without vortices. Interestingly, the plots indicate that significantly greater values of Nu_m can be obtained in the first region. In this region, it was determined that as the Richardson number increased, a slender continuous increase in the heat transfer rate was observed. However, surprisingly, it is indicated in Fig. 10 that for the minimum Reynolds number case examined ($Re = 80$), Nu_m had a small bell shape as it increased minimally until achieving a peak value and then decreased. Despite the fact that this trend of Nu_m disappears for greater Reynolds numbers ($Re > 80$), the rate of heat transfer monotonically increases. In fact, as eddies are formed and shed behind the circular cylinder, greater fluid mixing across the wake occurs, which in turn leads to an increased heat transfer. This result in this region is found to be opposite to that reported by Chang and Sa [30]. They determined that in the positive range of Richardson number $0 < Ri < 0.15$, the average Nusselt number decreased marginally to compose a localised minimum at the critical Richardson number of $Ri_{cr} = 0.15$.

Above the critical Richardson number, a sudden significant decrease in Nu_m is observed. This critical value marks the point at which vortex shedding is suppressed and the near wake reverts to a steady recirculating flow. It can be observed that the suppression of vortex shedding occurs for $Ri_{cr} \geq 0.09$ at.

$Re = 80$, and the value of the critical Richardson number increases as the Reynolds number increases. For example, it is noted that vortex shedding is suppressed for $Ri_{cr} \geq 0.09$, 0.14, 0.17, and 0.23 at $Re = 80$, 100, 120, and 150, respectively. This phenomena was observed previously in the experimental work of Noto and Matsumoto [48] for a heated circular cylinder situated in an upward fluid flow; they attributed this to "breakdown of the Kármán vortex street". It was also reported by Bhattacharyya et al. [49] for a square cylinder in the vicinity of a horizontal wall. Chang and Sa [30] found that the critical Richardson number is equal to 0.15 at a Reynolds number of 100.

In the second region, the response of the time-mean surface-averaged cylinder Nusselt number (Nu_m) to the increase in the Richardson number is indicated to be significantly different. Initially, a marginal increase in Nu_m is observed until it achieves a peak value. Then, a further increase in the Richardson number results in a notable decrease in Nu_m until it approaches a minimum value, prior to beginning to increase once again. This behaviour was not observed in the work of Chang and Sa [30]. They found that Nu_m increases considerably after the suppression of vortex shedding as the Richardson number increases for $Ri \geq 0.15$. In fact, physically, the behaviour of Nu_m in this region of the present study is due to the thermal boundary layer remaining attached to the cylinder leading to a higher temperature gradient leading to a higher rate of heat conveyance. These figures illustrate the dependence of the flow and thermal fields not only on the Richardson number but also on the Reynolds number. It can be observed that the second region represents a competition between buoyancy and forced convection for domination. Therefore, an increase in the Richardson number results in a considerable augmentation in Nu_m, and the dynamic field becomes more dominated by the buoyancy-induced convection flows. Further clarification of this behaviour is provided later when discussing the effect of the Richardson number on the temperature distribution in this region.

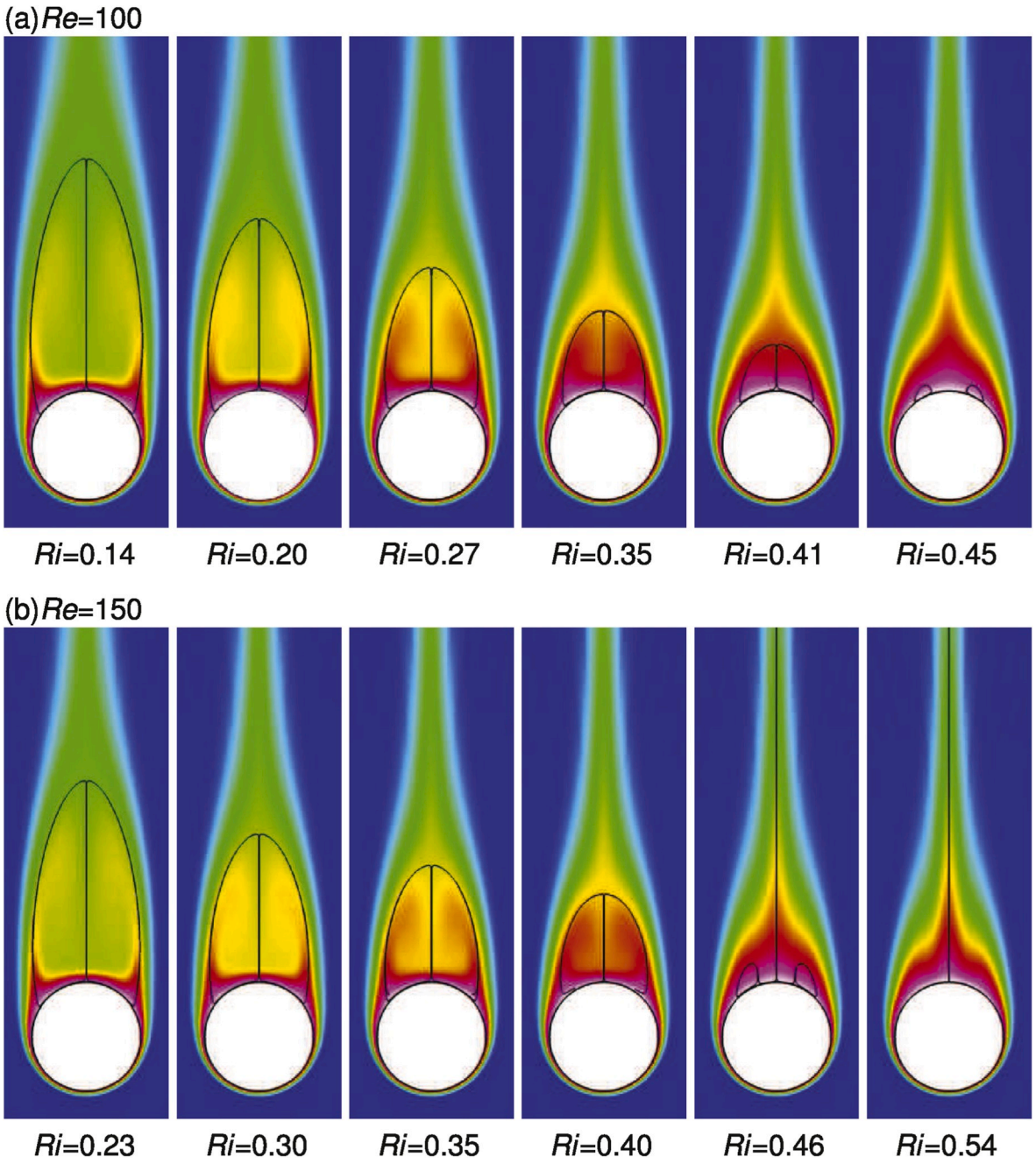

Fig. 16. Temperature distribution of steady flows with twin vortices about the cylinder for (a) $Re = 100$ and (b) $Re = 150$, at various Richardson number.

Figs. 12 and 13 display the influence of heating the cylinder surface on the streamflow field and temperature distribution with reference to vorticity, streamline, and isotherm patterns at a particular time for $Re = 100$ and 150. These distributions correspond to sets of Richardson number below the critical values at each respective Reynolds number. The streamlines indicate unsteady periodic behaviour for ($Ri < Ri_{cr}$). Thus, in the wake region, the two detached shear layers roll up to form negative and the positive eddies. Further downstream, the connection between the negative and positive vortices is eliminated, and the strengths of the vortices decrease owing to the viscous diffusion and cross-annihilation of vorticity, as they convect downstream. A comparison between the flow patterns for these values of $Ri > 0$ and those for an adiabatic cylinder ($Ri = 0$) demonstrates the influence of adding buoyancy. It reveals that the separation of the boundary layer occurs marginally earlier, and the vorticity increases minimally, which gives an apparent clarification for the average.

Nusselt number marginal increase in the periodic region.

Moreover, the isotherms for different Richardson numbers corresponding to a fixed Reynolds number, which represent the movement of heat, depict a cyclic behaviour as a consequence of the vibratory nature of the wake zone. Hence, as both hydrodynamic and thermal energy are conveyed by the fluid moving in this zone, the patterns of the isotherms and vorticity have several analogous features. In these figures, it can be observed that the symmetrical growth of the thermal boundary layer begins at the lower stagnation point of the cylinder and expands towards the upper stagnation point. For the downstream aspect, the effect of vortex shedding on the flow behaviour is clearly captured in the migration of the isotherms, whereas on the upstream part, the temperature distribution includes high thermal gradients. Therefore, the heat is demonstrated to be diffused throughout the flow field as localised warm

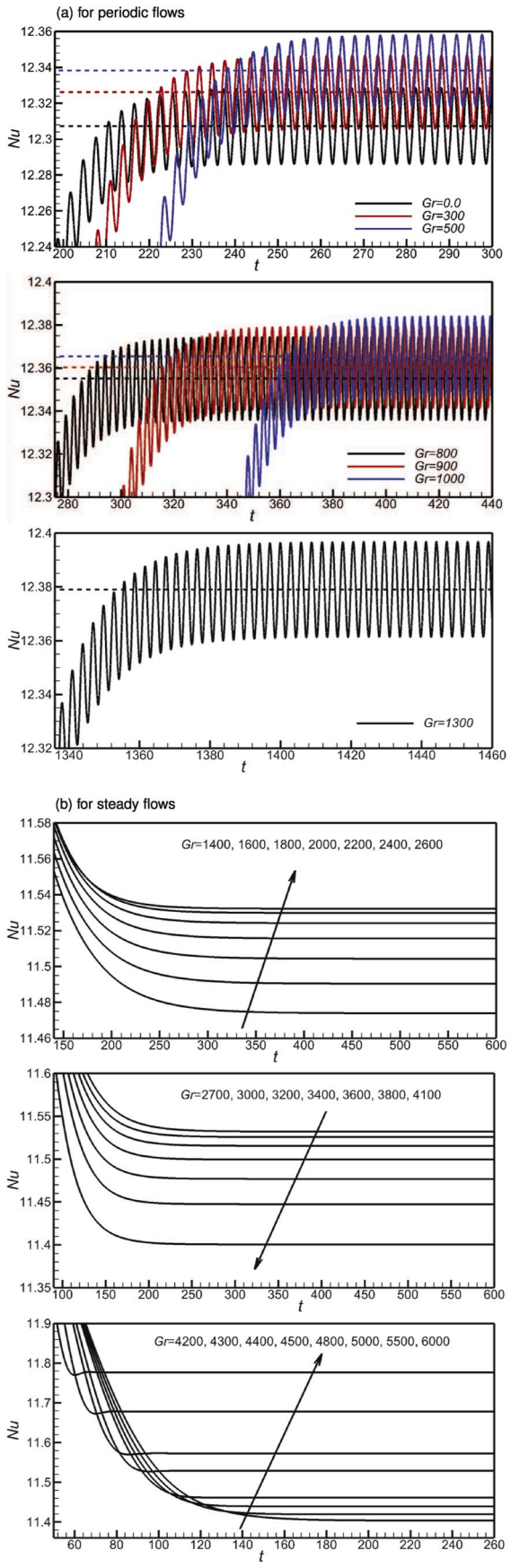

Fig. 17. (Cont.): The transient variation of Nusselt number for (a) periodic flows and (b) steady flows, for $Re = 100$, and at various Grashof number, showing the oscillating and consistent behaviours of Nu, respectively.

blobs. They are situated inside the vortex construction and move downward in the direction of the streamflow with the exception of being overly influenced by mixing with the surrounding environment.

Furthermore, at a constant Reynolds number, an increment in the Richardson number effectively corresponds to an increase in the cylinder wall temperature. It is clear from Figs. 14 and 15 that with increased heating, and above the critical value of the Richardson number (i.e. $Ri_{cr} = 0.13$ and 0.22 at $Re = 100$ and 150, respectively), buoyancy imparts stability to the wake region, and accordingly, the flow is observed to be completely steady. It then consists of twin stationary symmetric eddies of opposite-sign circulation. At the onset, these eddies are observed to develop more in size across and along the flow stream, making the wake considerably longer and wider than what was commonly recognised for typical shedding previously. As stated by Gerrard [50], for the case of flow over an isothermal cylinder, for vortices to shed, the wake chamber must open and compose immediate "alleyways" for fluid to permeate the chamber. However, for convective flow passed a hot cylinder, entrainment of cold fluid into the wake region declines and disappears beyond certain values of the critical Richardson number, resulting in a considerable deactivation of vortex shedding. Here, the streamline patterns reveal that the flow reversal and the size of the wake region are strongly dependent on the Richardson number. It was determined that for a certain Reynolds number, as the Richardson number increases, the recirculation region is reduced significantly, and at a particular value of the Richardson number (i.e. $Ri = 0.48$ and 0.54 at $Re = 100$ and 150, respectively), the flow circulating flow in the wake zone vanishes and the flow detachment occurs only at the backward stagnation point. This can be ascribed to the fact that for further heating, the buoyant forces are aiding the flow and accelerating it in the dynamic boundary layer, and hence has the effect of decreasing flow deceleration caused by the counter pressure gradient. This effect generates a considerable pressure reduction and creates regions of suction causing a detachment delay of the boundary layer.

The influence of the Richardson number on the temperature distribution about the cylinder wall in the steady region can be observed in Fig. 16 (a) and (b), at $Re = 100$ and 150, respectively. It should be noted that the thermal pattern of the heated cylinder is severely altered by the buoyant force. As can be observed, the growth of the thermal boundary layer commences approximately symmetrically beginning at the anterior surface of the cylinder, becoming wider towards the back. As the Richardson number increases, the fluid begins moving strongly along the cylinder surface in the upward direction from the anterior face towards the rear stagnation point. Consequently, the majority of the incoming accelerated fluid flows over the centreline of the cylinder. This strong upward motion induces a thermal plume in the vertical direction, which rises in the cylinder near-wake. In this thermal plume, the hot fluid stays beneath the cold fluid. It is important to note that for $Ri >$ 0.41 and $>$ 0.46 at $Re = 100$ and 150, respectively, this plume begins narrowing. Moreover, a higher thermal gradient in the proximity of the majority of the cylinder perimeter is apparent in the isotherm maps, except in the rear region. In particular, temperature contours are intensively and closely packed near the left and right sides of the cylinder.where separation would normally occur. This correlates with a significant cooling for the hot wall of the cylinder in these areas by the thermally accelerated boundary layer, which increases as Richardson number increases.

The low convective cooling in the front cylinder surface due to the lower thermal gradient decreases further as the Richardson number increases owing to the thermal plume formed. The counter-rotating cell generated at the start behind the cylinder slowly sweeps more warm fluid away from the cylinder wall. This is the evident clarification for the average Nusselt number behaviour in this region, i.e. marginally increases owing to the front higher thermal gradient and the existence of a circulating cell, and mildly decreases owing to the formation of the thermal plume, and then sharply increases after its minimum point owing to the shrinking of the thermal plume.

The transient variation of the Nusselt number (Nu) for periodic and steady flows at $Re = 100$ are displayed in Fig. 17 and (Cont.), respectively, for several values of Grashof number. The unsteady time-periodic behaviour of Nu can be observed in Fig. 17 for $Gr \leq 1300$ or $Ri \leq 0.13$, i.e. the Nu computed at the cylinder wall is altering at each instant during the vortex shedding cycle. It can also be observed that the shedding period is robustly reliant on the Richardson number. The figure clearly indicates that by increasing the Richardson number, the time necessary to achieve the fully periodic asymptotic state significantly increases. (In all cases, the simulations were started from the same initial conditions at time zero).

In the present investigation, the non-dimensionalised shedding frequency represented by Strouhal number, $St = fD/u_o$, is deduced from the signal traces of Nu to quantify the effect of the Richardson number on the frequency of vortex shedding. It was determined that increasing the Richardson number causes a monotonic improvement in both the frequency and amplitude of the vortex shedding. This is because the boundary layer over the sides and rear of the cylinder accelerates due to heating, causing a notable rise in the vortex shedding frequency and increased feeding of circulation into the wake. However, Fig. 17 (Cont.) indicates that for $Gr \geq 1400$ or $Ri \geq 0.14$, after a transient period, a steady Nu is obtained. It is clear that a shorter transient period is required to obtain steady-state values of Nu with a higher Richardson number.

5. Conclusion

A numerical study was performed to investigate the problem of mixed forced and natural convection from a heated circular cylinder subject to a vertical upward laminar flow of a viscous incompressible fluid. The influence of *assisting thermal buoyancy* on the flow and thermal fields in general, and on the collapse of vortex shedding, next to the cylinder in particular, for different ranges of Reynolds number, and Grashof or Richardson numbers, was considered. The results confirm that the natural eddy roll-up process that occurs over the chosen range of Reynolds number $80 \leq Re \leq 150$ is strengthened by buoyancy with a considerable augmentation in the time-mean and surface-average Nusselt number (Nu_m). This is expected, as a higher Richardson number amplifies the shedding amplitude and frequency and thus more frequent and intense vortices are shed, producing considerable augmentation in the heat transfer rates. However, the results reveal that the frequent vortex shedding in the backside of the cylinder vanishes completely and the dynamic wake is observed to degenerate into twin steady eddies after a particular critical value of Richardson number (Ri_{cr}), which is found to increase with the Reynolds number. It is noted that the vortex shedding is suppressed for $Ri_{cr} \geq 0.09$, 0.14, 0.17 and 0.23 at $Re = 80$, 100, 120, and 150, respectively. Interestingly, the current results illustrate that the buoyancy force does not always enhance the convection heat transfer rate above that for unadulterated forced convection. In particular, as the Richardson number is increased beyond its (Reynolds number dependent) critical values, shedding is suppressed and a sudden drop in the Nu_m occurs. Furthermore, the results confirm that the streamflow and thermal convection attributes of the stable wake downstream of the cylinder can be significantly changed by the superimposed thermal buoyancy, and the trend of Nu_m initially fluctuates prior to steadily increasing. This fluctuation is due to the competition between the forced convection front region of the cylinder and the buoyant thermal plume that forms behind the cylinder. The results also demonstrate that the vertical thermal plume spreads to a greater space after of the cylinder for larger values of Richardson number.

Declaration of competing interest

None.

Acknowledgement

This research was supported in part by the Monash eResearch Centre and eSolutions-Research Support Services through the use of the MonARCH HPC Cluster.

Appendix A. Supplementary data

Supplementary data to this article can be found online at https://doi.org/10.1016/j.ijthermalsci.2020.106434.

Funding

This research did not receive any specific grant from funding agencies in the public, commercial, or not-for-profit sectors.

References

[1] E. Bergere, R. Wille, Periodic flow phenomena, Annu. Rev. Fluid Mech. 41 (1) (1972) 313–340.
[2] C.H.K. Williamson, Vortex dynamics in the cylinder wake, Annu. Rev. Fluid Mech. 28 (1996) 477–539.
[3] G. Biswas, S. Sandip, Effect of thermal buoyancy on vortex shedding past a circular cylinder in cross-flow at low Reynolds numbers, Int. J. Heat Mass Tran. 52 (2009) 1897–1912.
[4] K. Ankit, K.D. Amit, Effect of a circular cylinder on separated forced convection at a backward-facing step, Int. J. Therm. Sci. 52 (2012) 176–185.
[5] W. Jiansheng, Z. Yunjian, Heat and fluid flow characteristics of a rectangular channel with a small diameter circular cylinder as vortex generator, Int. J. Therm. Sci. 92 (2015) 1–13.
[6] W. Jiansheng, W. Chen, Heat transfer and flow characteristics of a rectangular channel with a small circular cylinder having slit-vent vortex generator, Int. J. Therm. Sci. 104 (2016) 158–171.
[7] S.A. Kumar, S.A. Lal, A. Sameen, Flow past a moderately heated horizontal cylinder at low Reynolds number, J. Aero. Eng. 230 (2016) 1224–1239.
[8] S. Sumit, C. Dominic, Effects of thermal induced buoyancy forces on the vortex shedding of a circular cylinder, Int. Commun. Heat Mass Tran. 76 (2016) 215–224.
[9] S.D. Vivien, N.S. Ahmad, R. Syaiful, Numerical study of mixed convection around a heated circular cylinder, Appl. Mech. Mater. 836 (2016) 85–89.
[10] A.I. Aleksyuk, A.N. Osiptsov, Direct numerical simulation of energy separation effect in the near wake behind a circular cylinder, Int. J. Heat Mass Tran. 119 (2018) 665–677.
[11] D. Amit, G. Rishabh, B. Lszl, Cross-buoyancy mixed convection from a heated cylinder placed asymmetrically in a channel, Int. Commun. Heat Mass Tran. 95 (2018) 139–146.
[12] B. Sonal, K. Harshit, D. Amaresh, S. Sandip, Effect of channel confinement on wake dynamics and forced convective heat transfer past a blunt headed cylinder, Int. J. Therm. Sci. 124 (2018) 467–476.
[13] L. Zheng, X. Xianchen, L. Kuojiang, C. Yangyang, H. Guoliang, C. Chung-Lung, C. Chien-Hua, Airfoil-shaped self-agitator for convective heat transfer enhancement, Int. J. Therm. Sci. 133 (2018) 284–298.
[14] P. Oosthuizen, S. Madan, Combined convection heat transfer from horizontal cylinders in air, Trans. ASME J. Heat Trans. 92 (1970) 194–196.
[15] T. Jackson, H. Yen, Combined forced and free convective equations to represent combined heat transfer coefficients for horizontal cylinders, Trans. ASME J. Heat Trans. 93 (1971) 247–248.
[16] A. Acrivos, On the combined effect of forced and free convection heat transfer in laminar boundary layer flows, Chem. Eng. Sci. 21 (4) (1966) 343–352.
[17] N. Joshi, S. Sukhatme, An analysis of combined free and forced convection heat transfer from a horizontal circular cylinder, Trans. ASME J. Heat Trans. 93 (1971) 441–448.
[18] S. Nakai, T. Okazaki, Heat transfer from a horizontal circular wire at small Reynolds and Grashof numbers, Int. J. Heat Mass Tran. 18 (1975) 397–413.
[19] E. Sparrow, L. Lee, Analysis of mixed convection about a horizontal cylinder, Int. J. Heat Mass Tran. 19 (1976) 229–232.
[20] J.H. Merkin, Mixed convection from a horizontal circular cylinder, Int. J. Heat Mass Tran. 20 (1977) 73–77.
[21] H.M. Badr, Laminar combined convection from a horizontal cylinder-parallel and contra flow regimes, Int. J. Heat Mass Tran. 27 (1) (1984) 15–27.
[22] H.M. Badr, On the effect of flow direction on mixed convection from a horizontal cylinder, Int. J. Numer. Methods Fluid. 5 (1985) 1–12.
[23] A. Syakila, M. Norihan, N. Roslinda, P. Ioan, Mixed convection boundary layer flow past an isothermal horizontal circular cylinder with temperature-dependent viscosity, Int. J. Therm. Sci. 48 (2009) 1943–1984.
[24] P. Jain, B. Lohar, Unsteady mixed convection heat transfer from a horizontal circular cylinder, Trans. ASME J. Heat Trans. 101 (1979) 126–131.
[25] K. Noto, R. Matsumoto, Numerical simulation on development of the karmanvortex street due to the negative buoyancy force, in: Numerical Methods in Laminar and Turbulent Flow, vol. 5, 1987, p. 796.

[26] B. Farouk, S. Guceri, Natural and mixed convection heat transfer around a horizontal cylinder within confining walls, Numer. Heat Tran. 5 (3) (1982) 329–341.
[27] C. Ho, M. Wu, J. Jou, Analysis of buoyancy aided convection heat transfer from a horizontal cylinder in a vertical duct at low Reynolds number, Wrme-und Stoffbertragung 25 (6) (1990) 337–343.
[28] S. Singh, G. Biswas, A. Mukhopadhyay, Effect of thermal buoyancy on the flow through a vertical channel with a built-in circular cylinder, Numer. Heat Tran. 34 (1998) 769–789.
[29] G. Gandikota, S. Amiroudine, D. Chatterjee, G. Biswas, The effect of aiding/opposing buoyancy on two-dimensional laminar flow across a circular cylinder, Numer. Heat Tran. 58 (5) (2010) 385–402.
[30] K. Chang, J. Sa, The effect of buoyancy on vortex shedding in the near wake of a circular cylinder, J. Fluid Mech. 220 (1990) 253–266.
[31] K. Hatanaka, M. Kawahara, Numerical study of vortex shedding around a heated/cooled circular cylinder by the three-step Taylor-Galerkin method, Int. J. Numer. Methods Fluid. 21 (1995) 857–867.
[32] G. Karniadakis, G. Triantafyllou, Three-dimensional dynamics and transition to turbulence in the wake of bluff objects, J. Fluid Mech. 238 (1992) 1–30.
[33] A. Tomboulides, G. Triantafyllou, G. Karniadakis, A New mechanism of period doubling in free shear flows, Phys. Fluids 4 (1992) 1329–1332.
[34] M.C. Thompson, K. Hourigan, A. Cheung, T. Leweke, Hydrodynamics of a particle impact on a wall, Appl. Math. Model. 30 (2006) 1356–1369.
[35] C.S. Peskin, Flow patterns around heart valves: a numerical method, J. Comput. Phys. 10 (2) (1972) 252–271.
[36] G.E. Karniadakis, S.J. Sherwin, Spectral/hp Methods for Computational Fluid Dynamics, Oxford University Press, Oxford, 2005.
[37] M.C. Thompson, K. Hourigan, J. Sheridan, Three-dimensional instabilities in the wake of a circular cylinder, Exp. Therm. Fluid Sci. 12 (1996) 190–196.
[38] G. Al-Sumaily, S. John, M.C. Thompson, Analysis of forced convection heat transfer from a circular cylinder embedded in a porous medium, Int. J. Therm. Sci. 51 (2012) 121–131.
[39] G. Al-Sumaily, M.C. Thompson, Forced convection from a circular cylinder in pulsating flow with and without the presence of porous media, Int. J. Heat Mass Tran. 61 (2013) 226–244.
[40] G. Al-Sumaily, Forced convection heat transfer from a bank of circular cylinders embedded in a porous medium, J. Heat Trans. ASME 136 (4) (2014), 042602–042602–11.
[41] G. Al-Sumaily, M.C. Thompson, Bnard convection from a circular cylinder in a packed bed, Int. Commun. Heat Mass Tran. 54 (2014) 18–26.
[42] K. Nasr, S. Ramadhyani, R. Viskanta, Experimental investigation on forced convection heat transfer from a cylinder embedded in a packed bed, J. Heat Tran. 116 (1) (1994) 73–80.
[43] P. Cheng, Mixed convection about a horizontal cylinder and a sphere in a fluid-saturated porous medium, Int. J. Heat Mass Tran. 25 (8) (1982) 1245–1247.
[44] E. Buyruk, Numerical study of heat transfer characteristics on tandem cylinders, inline and staggered tube banks in cross-flow of air, Int. Commun. Heat Mass Tran. 29 (3) (2002) 355–366.
[45] K. Noto, T. Nakajima, Wake instability behind a circular cylinder at the low Reynolds number, in: Proceedings of 5th International Symposium on Computational Fluid Dynamics, vol. 2, 1993, p. 369374.
[46] M.M. Zdravkovich, Flow Around Circular Cylinders, ume 1, Oxford University Press, Oxford, 1997.
[47] J. Dusek, P. Le Gal, D. Fraunie, A numerical and theoretical study of the first Hopf bifurcation in a cylinder wake, J. Fluid Mech. 264 (1994) 59–80.
[48] K. Noto, R. Matsumoto, A breakdown of the karman vortex street due to the natural convection. Proceedings of the International Symposium on Flow Visualisation, Springer-Verlag, Berlin, 1985, pp. 348–354.
[49] S. Bhattacharyya, D. Maiti, S. Dhinakaran, Influence of buoyancy on vortex shedding and heat transfer from a square cylinder in proximity to a wall, Numer. Heat Tran. 50 (2006) 585–606.
[50] J.H. Gerrard, The mechanics of the vortex formation region of vortices behind bluff bodies, J. Fluid Mech. 25 (1966) 401–413.